yarn (1 for each different yarn type, plus the average number of yarn components, plus values from 0 to 4 assigned for the average amount of yarn twist), and fiber (1 for each different fiber type used plus values from 1 to 4 assigned for the average amount of fiber preparation or processing).

9. S. C. Scholtz, *Prehistoric Piles: A Structural and Comparative Analysis of Cordage, Netting, Basketry and Fabric from Ozark Bluff Shelters* (Arkansas Archeological Research Series 9, Arkansas Archeological Survey, Fayetteville, AR, 1975).
10. K. J. Gremillion, K. Jakes, V. Wimberley, paper presented at the Kentucky Heritage Council Annual Meeting, Natural Bridge State Park, KY, 14 to 16 March 1997; M. E. King, in *Archaeology of the Mammoth Cave Area*, P. J. Watson, Ed. (Academic Press, New York, 1974), pp. 31–40; J. Miller, *Southeast. Archaeol.* **7**, 132 (1988); W. Orchard, *Sandals and Other Fabrics from Kentucky Caves* (Indian Notes and Monographs 4, Museum of the American Indian, Heye Foundation, New York, 1920); P. J. Watson, *Prehistory of Salts Cave, Kentucky* (Reports of Investigations 16, Illinois State Museum, Springfield, IL, 1969).
11. K. Kankainen, Ed., *Treading In the Past: Sandals of the Anasazi* (Utah Museum of Natural History and the Univ. of Utah Press, Salt Lake City, UT, 1995).
12. M. B. Collins, *Test Excavations at Amistad International Reservoir Fall, 1967* (Papers of the Texas Archaeological Salvage Project 16, Austin, TX, 1969); J. A. Word and C. L. Douglas, *Excavations at Baker Cave, Val Verde County, Texas* (Bulletin 16, Texas Memorial Museum, Austin, TX, 1970).
13. N. J. Hewitt, in *Cowboy Cave*, J. Jennings, Ed. (Anthropological Papers 10, University of Utah, Salt Lake City, UT, 1980), pp. 49–74.
14. S. F. Bedwell, *Fort Rock Basin, Prehistory and Environment* (Univ. of Oregon Books, Eugene, OR, 1973).
15. L. S. Cressman, *Southwest. J. Anthropol.* **7**, 289 (1951); L. S. Cressman, *Prehistory of the Far West, Homes of Vanished Peoples* (Univ. of Utah Press, Salt Lake City, UT, 1977).
16. P. R. Geib, *Utah Archaeol.* **9**, 35 (1996).
17. The Pretoria calibration procedure program by Beta Analytic, Inc. was used.

18. We thank D. Glover for technical assistance, C. White for photography, M. Standifer for fiber identification, E. J. O'Brien for editorial advice, and R. L. Lyman for references. Funding for AMS dating was provided by the College of Arts and Science, University of Missouri–Columbia.

19 March 1998 accepted; 8 May 1998

Dissociative Recombination of HD⁺ in Selected Vibrational Quantum States

Z. Amitay, A. Baer, M. Dahan, L. Knoll, M. Lange, J. Levin, I. F. Schneider, D. Schwalm, A. Suzor-Weiner, Z. Vager, R. Wester, A. Wolf, D. Zajfman*

Rate coefficients for dissociative recombination of HD^+ in selected vibrational states have been measured by a combination of two molecular fragment imaging methods by using the heavy-ion storage ring technique. Recombination fragment imaging yields state-to-state reaction rates. These rates are converted to rate coefficients by using vibrational level populations of the stored ion beam, derived from nuclear coordinate distributions measured on extracted ions. The results show strongly increasing rate coefficients for high vibrational excitation, where additional dissociation routes open up, in agreement with a theoretical calculation. Very low rate coefficients are found for certain, isolated vibrational states.

The last 20 years have seen tremendous progress in our understanding of elementary chemical reactions. Molecular-beam experiments have provided very detailed information about the dynamics of inelastic and reactive collisions (*1*). Supersonic expansion, which leads to a strong reduction of the temperature relevant for the molecular level population, has been widely exploited to analyze neutral molecules in their vibrational ground state. Much greater experimental difficulties are encountered in producing molecules and molecular ions in well-defined excited states, and studies of their collision dynamics, important in such areas as high-temperature combustion media or atmospheric processes under nonequilibrium conditions (*2*), are scarce.

Dissociative recombination (DR) (*3*) of molecular ions with free electrons is an elementary reactive collision that is highly sensitive to vibrational excitation. In many partly ionized gas-phase environments, the process removes charged particles and produces neutral fragments carrying considerable kinetic energy and often also internal excitation. The process is therefore very important in astrophysics and planetary science; for example, the DR of O_2^+ molecules is responsible for the production of the so-called green-light emission (airglow) in Earth's ionosphere (*4, 5*).

The detailed understanding of the DR process has suffered from the lack of knowledge about the internal excitation of laboratory molecular ion beams, which has made comparison between experimental results and theory difficult (*6*). Techniques have been developed during the last 5 years that use molecular ions in heavy-ion storage rings, which relax to their vibrational ground state within several seconds of storage time. Cross sections of DR were measured with this method for a variety of important species after relaxation to the vibrational ground state (*7*). These measurements with vibrationally cold molecular ions revealed structures in the DR cross section that resulted from unexpected recombination mechanisms (*8, 9*); in combination with two- and three-dimensional molecular fragment imaging techniques (*10*), the contributions for well-defined final quantum states of the fragments could be measured. Advanced theoretical calculations yielded good agreement with the data for ions in the vibrational ground state (*11*).

For the experimental approach used here the storage ring technique was extended to yield reaction rate coefficients for vibrationally excited molecular ions during their relaxation. The fragment imaging method allows us to determine relative reaction rates for molecular ions in excited states with vibrational quantum numbers v ranging from 0 to 7; by the simultaneous identification of the final fragment levels, it basically yields state-to-state reaction rates. This powerful technique is combined with an independent method for measuring the vibrational state distribution in the stored, relaxing beam, which uses Coulomb explosion imaging (CEI) (*12, 13*) of molecular ions extracted from the ring; the measured recombination rates for the different initial states can thus be converted into rate coefficients, which can be directly compared with theory.

A reaction well suited for initiating these studies is the DR of HD^+ with low-energy electrons (experimental energy spread ~10 meV). HD^+ is the simplest molecular ion subject to vibrational relaxation by infrared emission. Its DR with low-energy electrons can be depicted as

$$HD^+(v) + e^- \rightarrow \begin{matrix} H(1s) + D(nl) \\ \text{or} \\ H(nl) + D(1s) \end{matrix} \qquad (1)$$

where nl denotes the orbital of the electron in the atomic fragments. Starting with the capture of an electron by the molecular ion, a rearrangement of the whole electronic cloud leads to a transfer of kinetic energy to the

---

Z. Amitay, A. Baer, M. Dahan, J. Levin, Z. Vager, D. Zajfman, Department of Particle Physics, Weizmann Institute of Science, Rehovot, 76100, Israel. L. Knoll, M. Lange, D. Schwalm, R. Wester, A. Wolf, Max-Planck-Institut für Kernphysik and Physikalisches Institut der Universität Heidelberg, D-69029 Heidelberg, Germany. I. F. Schneider and A. Suzor-Weiner, Laboratoire de Photophysique Moléculaire, Université Paris XI, 91405 Orsay, France, and National Institute of Lasers, Plasma and Radiation Physics, Post Office Box MG-36, 76900 Bucharest-Magurele, Romania.

*To whom correspondence should be addressed. E-mail: fndaniel@wicc.weizmann.ac.il

dissociating nuclei. The DR from lower lying vibrational states v of HD$^+$ predominantly starts by electron capture in the $^1\Sigma_g^+$ doubly excited, dissociating state of neutral HD (Fig. 1). This state crosses all the vibrational levels of HD$^+$ at different locations. The recombination rate therefore strongly depends on the vibrational excitation of the ion. For higher vibrational excitation, an additional effect involving the next $^3\Pi_g$ dissociative curve and higher dissociative Rydberg states can be expected. Figure 1 also illustrates that measurement of the kinetic energy release E_k identifies both the initial and the final state of the reaction.

The experiment was carried out at the Max-Planck-Institut für Kernphysik, Heidelberg, Germany with the Test Storage Ring (TSR) (*14*). A 2.0-MeV HD$^+$ beam produced by a standard Penning ion source was injected into the TSR; typically 10^7 particles circulated in the ring with a lifetime of $\sim$10 s. The vibrational cooling time of HD$^+$ is $\sim$300 ms, depending on the initial vibrational excitation created in the ion source. The circulating beam was merged with a 3.5-cm-diameter, quasimonochromatic electron beam over a length of 1.5 m, providing electrons at a typical density of 2×10^6 cm^{-3} and a temperature of 10 meV in the comoving reference frame. Recombination fragments produced in this interaction region were detected as a function of the storage time t by using an imaging microchannel plate located 6 m downstream (*10*). Both the state-specific recombination rates $r_v(t)$ and the level populations $N_v(t)$ were measured as a function of storage time from injection ($t = 0$) to complete relaxation ($t > 300$ ms), thus probing a manifold of vibrational state distributions. The combination of these results then yields the DR rate coefficient α_v for molecular ions in a vibrational state v as

$$\alpha_v = K r_v(t)/N_v(t) \qquad (2)$$

with a normalization constant K independent of t and v. This experiment aims to determine rate coefficients relative to $\alpha_{v=0}$, therefore absolute normalizations of $r_v(t)$ and $N_v(t)$ are not required.

The two-dimensional molecular fragment imaging technique (*10*) reveals the relative recombination rates for different amounts of kinetic energy release E_k (and thus the state-specific reaction rates). The two atomic fragments produced in a recombination process move relative to each other according to the energy release E_k, and their transverse distance D on arrival at the detector is measured event by event. The random orientations of the internuclear axis and the random positions of the event vertices within the interaction region result in a distribution of the projected distances. For a given E_k, the distribution rises from zero at $D = 0$ to a peak at distance D_1 (molecules dissociating perpendicular to the beam direction at an interaction point lying closest to the detector) and then decreases again with an edge at the maximal distance D_2 (perpendicular orientation and most distant interaction point); both D_1 and D_2 vary as $\propto \sqrt{E_k}$. Usually contributions for different E_k add up in the total distribution (*10*).

Projected distance distributions for the DR of HD$^+$ were measured for different storage times, corresponding to different vibrational state populations (Fig. 2, A to C). For vibrational states $v \leq 5$, only the final electronic states with $n = 2$ are energetically accessible (Fig. 1); here, increasing vibrational excitation just yields larger projected distances. For $v > 5$, the $n = 3$ state is also open, so that at short storage time, when the molecular ions are highly excited, many dissociations with a small value of D are observed (Fig. 2A). This part of the distribution rapidly decreases with time as the molecular ions cool down, and finally (Fig. 2C) the distribution for only a single value of E_k is obtained, as expected for $v = 0$, $n = 2$.

Using analytic functions (*10*) for the projected distance distribution, we fit the data accumulated for each time bin by a superposition of components for different E_k. As seen in Fig. 2B, each of the components contributes to the distribution in well-separated regions so that unambiguous results for their relative size and thus for the state-specific rates $r_v(t)$ could be obtained.

During the storage time, a small fraction of the beam was extracted from the TSR toward a new beam line, where the vibrational state distribution was measured with the CEI method. In this method, the fast molecular ions impinge on a very thin target (70 Å thick) and are stripped of their electrons. At 2-MeV beam energy, the stripping and dwell time in the foil are much shorter than the natural rotation-vibration time of the molecular ions; therefore, the internuclear distance R between the two bare nuclei is left unchanged by the stripping process, except for a small smearing effect as a result of multiple scattering of the projectile nuclei with the target atoms (*15*). After passing through the foil, the two bare nuclei repel each other through strong Coulomb repulsion, and their relative distance increases as the potential energy is transformed into kinetic energy in the center-of-mass frame of reference. We determined this kinetic energy E by three-dimensional imaging of each event, measuring the relative distance and the times of impact of the two fragments. The distribution of initial internuclear distances, $P_R(R;\ t)$, derived from the data with the simple Coulomb law

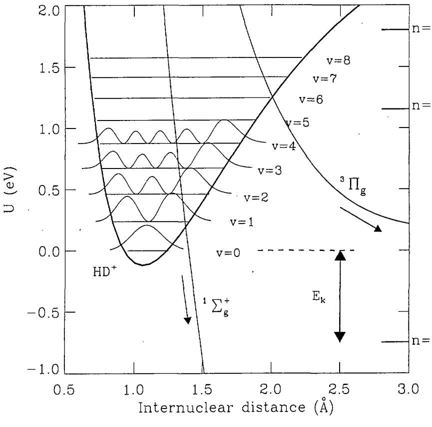

Fig. 1. Curves of the potential energy (U) for HD and HD$^+$, showing the electronic ground state of HD$^+$ together with the $v = 0$ to 4 vibrational wave functions. The two lowest of the doubly excited dissociative states of HD ($^1\Sigma_g^+$ and $^3\Pi_g$) responsible for the DR of HD$^+$ at low energy are shown. The bars on the right mark the asymptotic energy for the principal quantum number n of one of the fragments.

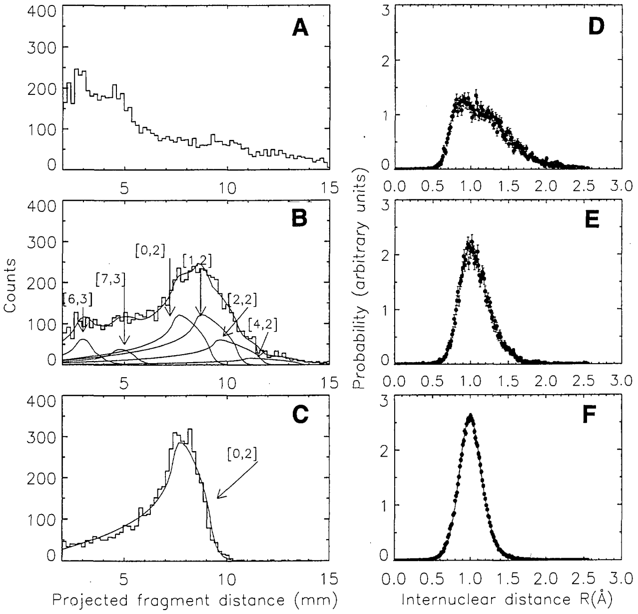

Fig. 2. (**A** to **C**) Projected distance distribution as measured for the DR of HD$^+$ at different storage times t: (A) 10 ms $< t <$ 20 ms; (B) 90 ms $< t <$ 100 ms; and (C) 440 ms $< t <$ 450 ms. The overall fits of the distributions are shown for (B) and (C), and the individual contributions (v, n) are shown for the intermediate time interval. (**D** to **F**) Internuclear distance distribution $P_R(R;\ t)$ of HD$^+$ as measured with the CEI technique for similar storage times: (D) 10 ms $< t <$ 20 ms; (E) 90 ms $< t <$ 100 ms; and (F) $t >$ 400 ms. For the long-time storage (F), the solid line represents the convoluted vibrational wave function squared of HD$^+$ in the $v = 0$ state.

$E(R) = e^2/R$, ideally represents the superposition of the squared vibrational wave functions $\Psi_\nu^2(R)$ of HD$^+$ according to

$$P_R(R;t)dR = \sum_\nu N_\nu(t)\Psi_\nu^2(R)dR \qquad (3)$$

The experimentally derived distributions $P_R(R;t)$ are broadened as a result of multiple scattering by only 10 to 20%. For short storage time (10 ms $< t <$ 20 ms), the distribution of internuclear distances is very wide (Fig. 2D) as a result of the broad distribution of vibrational states populated on injection. After 400 ms, this distribution has become narrow and no longer depends on the storage time (Fig. 2F). The molecular ions have cooled down to $\nu = 0$, and the measured distribution can be compared directly to the square of the ground-state vibrational wave function, $\Psi_0^2(R)$, of HD$^+$. A Monte-Carlo algorithm (*15*) was used to calculate the experimental R distribution, as influenced by multiple scattering, assuming the known wave function $\Psi_0^2(R)$; this yields very good agreement regarding the shape. At shorter times, distributions obtained by the same method for arbitrary ν were fitted with the relative populations $N_\nu(t)$ as the only free parameters. The time evolution of the experimentally derived vibrational populations can be compared with calculated populations (Fig. 3A). The calculations assume a vertical transition during electron impact ionization in the ion source from the ground state of HD to HD$^+$ and use theoretical radiative lifetimes of the vibrational states (*16, 17*). Both the observed initial vibrational state distribution and its temporal evolution confirm these simple theoretical predictions.

To obtain the rate coefficients according to Eq. 2, we used the time-dependent populations $N_\nu(t)$. The state-specific recombination rates $r_\nu(t)$ obtained from the DR fragment imaging measurement then yield relative rate coefficients (Fig. 3B), which we found to be time independent within the statistical errors. Suitable mean values (shown as straight lines) were extracted as the final experimental results. Contributions to the error bars from systematic errors due to different fitting procedures were also taken into account. The results are shown together with the present theoretical predictions in Fig. 4, which also include the previous theoretical results by Takagi (*18*) and Nakashima *et al.* (*19*). Our calculation and Takagi's results are for the experimental electron energy distribution, whereas Nakashima's results hold for a Maxwellian of 100 K. The theory we present here is based on the multichannel quantum defect method (*20*) and is the only one to take into account the higher energy dissociative curves (such as the $^3\Pi_g$ state shown in Fig. 1), allowing the rate coefficients to be calculated for vibrational quantum numbers up to 10. The overall trend of the theory is compatible with the experimental results in the sense that the DR rate coefficients for high vibrational states $\nu > 5$ are considerably larger than those for the lower states; the experimental relative rate coefficients of 15 to 40 for $\nu = 6$ and 7 are well reproduced. Hence, the new dissociation routes opening up for the higher ν states are in fact very efficient in increasing the recombination rate.

For the low vibrational states, a large spread exists among the different theoretical predictions as well as between these and the experimental results. One possible reason for such discrepancies is the slightly different $^1\Sigma_g^+$ dissociative curves used in the various calculations. Indeed, the main factor affecting the DR rates for these states is the Franck-Condon overlap between the initial vibrational state and the lowest dissociative state (Fig. 1). For example, the low experimental value for $\nu = 3$ is reproduced by the calculation of Nakashima *et al.* (*19*), who explicitly attributed the low value to a very poor Franck-Condon overlap. In general, the calculations succeed to reproduce some but not all of the measured values.

For the high vibrational states, the strong increase of the recombination rate predicted already for $\nu = 5$ is experimentally observed only for $\nu \geq 6$, whereas for $\nu = 5$ a particularly low value is found. In this case, we saw no major differences when we repeated our calculations using different sets of calculated potential curves; we could not reproduce the experimental value for $\nu = 5$. An interesting feature of the $\nu = 5$ state is that it lies just below the opening of the $n = 3$ atomic limit (Fig. 1). Part of the dissociating flux (through the $^3\Pi_g$ curve and higher dissociative states) could be directed toward this (closed) limit through diabatic transitions at an avoided crossing located at large internuclear distance and then redirected adiabatically to the autoionization region, which would result in a decrease of the DR rate for this specific state. The influence of such large-distance, avoided crossings is not taken into account in many molecular calculations because of insufficient knowledge of electronic interactions in this region.

The recombination rates for selected vibrational states we obtained here demonstrate the need for further theoretical work to understand the influence of vibrational excitation on the DR process and can be expected to guide future quantum chemistry calculations. The experimental technique is general and does not depend on specific level schemes, which are required for laser manip-

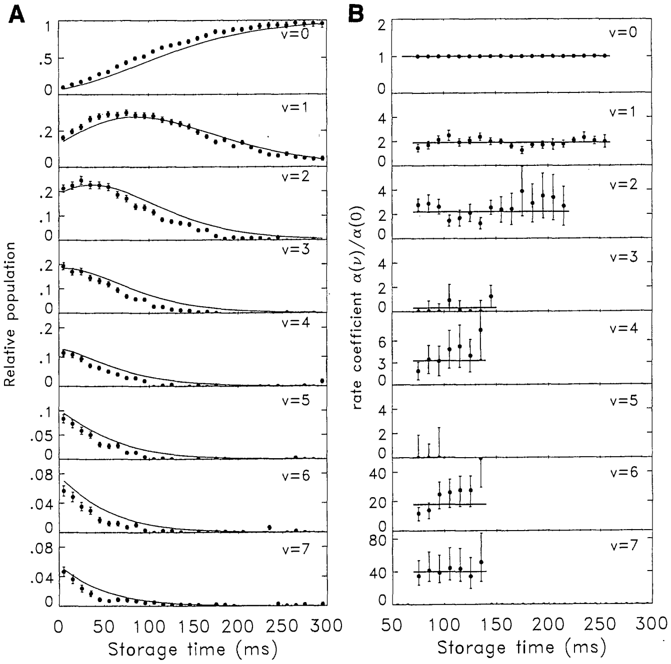

Fig. 3. (**A**) Time evolution of the vibrational state population ($0 \leq \nu \leq 7$) as obtained by fitting the $P_R(R;t)$ distributions. The solid line is the relative population as obtained with the assumption of an initial Franck-Condon population and theoretical lifetimes (*16, 17*). (**B**) DR relative rate coefficients for the various vibrational states for the different time bins. The horizontal lines represent the average value used as final values.

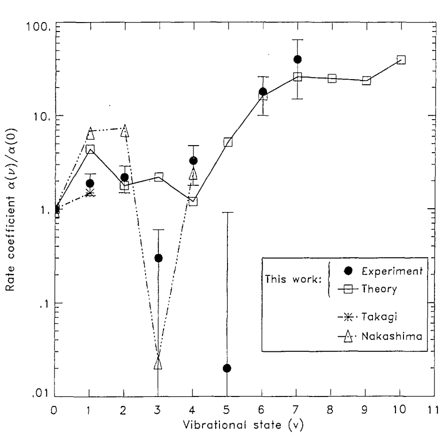

Fig. 4. DR relative rate coefficients as a function of vibrational quantum number. Both experiment and theories are normalized to unity for $\nu = 0$. The lines are drawn to guide the eye only.

ulation of vibrational states. The only requirements are the knowledge of the vibrational wave function and a vibrational cooling time that is shorter than the usable lifetime of the ions in a storage ring. Most heteronuclear molecular ions satisfy this criterion.

References and Notes

1. *Atomic and Molecular Beam Methods*, G. Scoles, Ed. (Oxford Univ. Press, New York, 1988).
2. T. G. Slanger, L. E. Jusinski, G. Black, G. E. Gadd, *Science* **241**, 945 (1988).
3. J. N. Bardsley and M. A. Biondi, *Adv. Mol. Phys.* **6**, 1 (1970).
4. D. Kella, L. Vejby-Christensen, P. J. Johnson, H. B. Pedersen, L. H. Andersen, *Science* **276**, 1530 (1997).
5. S. L. Guberman, *ibid.* **278**, 1276 (1997).
6. J. B. A. Mitchell, *Phys. Rep.* **186**, 215 (1990).
7. M. Larsson, *Annu. Rev. Phys. Chem.* **48**, 151 (1997), and references therein.
8. P. Forck *et al.*, *Phys. Rev. Lett.* **72**, 2002 (1994).
9. J. R. Mowat *et al.*, *ibid.* **74**, 50 (1995).
10. Z. Amitay *et al.*, *Phys. Rev. A* **54**, 4032 (1996).
11. C. Strömholm *et al.*, *ibid.* **52**, 4320 (1995).
12. Z. Vager, R. Naaman, E. P. Kanter, *Science* **244**, 426 (1989).
13. D. Zajfman and Z. Amitay, *Phys. Rev. A* **52**, 839 (1995).
14. D. Habs *et al.*, *Nucl. Instrum. Methods* **B43**, 390 (1989).
15. D. Zajfman, T. Graber, E. P. Kanter, Z. Vager, *Phys. Rev. A* **46**, 194 (1992).
16. M. Tadjeddine and G. Parlant, *Mol. Phys.* **33**, 1797 (1977).
17. Z. Amitay, D. Zajfman, P. Forck, *Phys. Rev. A* **50**, 2304 (1994).
18. H. Takagi, in *Dissociative Recombination: Theory, Experiment and Applications III*, D. Zajfman, J. B. A. Mitchell, D. Schwalm, B. R. Rowe, Eds. (World Scientific, Singapore, 1996), pp. 174–183.
19. K. Nakashima, H. Takagi, H. Nakamura, *J. Chem. Phys.* **86**, 726 (1987).
20. A. Giusti-Suzor, *J. Phys. B* **13**, 3687 (1980); S. Guberman and A. Giusti-Suzor, *J. Chem. Phys.* **95**, 2602 (1991).
21. Supported in part by the German Federal Minister for Education, Science, Research and Technology under contract number 06 HD 854I, by the Human Capital and Mobility Programme of the European Community, and by the German Israel Foundation under contract number I-0452-200.07/95.

3 March 1998; accepted 13 May 1998

An Inverted Hexagonal Phase of Cationic Liposome–DNA Complexes Related to DNA Release and Delivery

Ilya Koltover, Tim Salditt,* Joachim O. Rädler,† Cyrus R. Safinya‡

A two-dimensional columnar phase in mixtures of DNA complexed with cationic liposomes has been found in the lipid composition regime known to be significantly more efficient at transfecting mammalian cells in culture compared to the lamellar (L_α^C) structure of cationic liposome–DNA complexes. The structure, derived from synchrotron x-ray diffraction, consists of DNA coated by cationic lipid monolayers and arranged on a two-dimensional hexagonal lattice (H_{II}^C). Two membrane-altering pathways induce the $L_\alpha^C \rightarrow H_{II}^C$ transition: one where the spontaneous curvature of the lipid monolayer is driven negative, and another where the membrane bending rigidity is lowered with a new class of helper-lipids. Optical microscopy revealed that the L_α^C complexes bind stably to anionic vesicles (models of cellular membranes), whereas the more transfectant H_{II}^C complexes are unstable and rapidly fuse and release DNA upon adhering to anionic vesicles.

Complexes consisting of DNA mixed with oppositely charged cationic liposomes (CLs; closed bilayer membrane shells of lipid molecules) mimic natural viruses in their ability to act as synthetic carriers of extracellular DNA across outer cell membranes and nuclear membranes for gene delivery (*1–3*). The use of nonviral rather than viral methods for gene delivery has several advantages, including nonimmunicity and the potential for transferring and expressing (transfecting) large pieces of DNA into cells. Partial sections of first-generation human artificial chromosomes (HACs) on the order of 1 Mbp can be transferred into cells by means of CLs, although extremely inefficiently (*4*). The low transfection efficiencies of nonviral delivery methods may be improved through insights into transfection-related mechanisms at the molecular and self-assembled levels.

The efficiency of transfection mediated by mixtures of cationic lipids and so-called neutral "helper-lipids" varies widely and unpredictably (*1, 3, 5*). The choice of the helper-lipid has been empirically established to be important; for example, transfection of mammalian cells in culture is efficient in mixtures of the univalent cationic lipid DOTAP (dioleoyl trimethylammonium propane) and the neutral helper-lipid DOPE (dioleoyl phosphatidylethanolamine), and not in mixtures of DOTAP and a similar helper-lipid, DOPC (dioleoyl phosphatidylcholine) (*6*). We recently showed that mixing DNA with CLs consisting of DOPC and DOTAP leads to a topological transition into condensed CL-DNA complexes with a multilamellar structure (L_α^C), with DNA monolayers sandwiched between cationic lipid bilayers (*7*) in a manner similar to the schematic in Fig. 1 (left).

Using synchrotron small-angle x-ray scattering (SAXS) and optical microscopy, we found a completely different columnar inverted hexagonal H_{II}^C liquid-crystalline state in CL-DNA complexes (Fig. 1, right). The commonly used helper-lipid DOPE induces the $L_\alpha^C \rightarrow H_{II}^C$ structural transition by controlling the spontaneous curvature $C_o = 1/R_o$ of the lipid monolayer, where R_o is the natural radius of curvature (Fig. 1, pathway I). We also identified a class of helper molecules that control the membrane bending rigidity κ and give rise to a second pathway to the H_{II}^C phase (Fig. 1, pathway II). The CL-DNA complexes containing DOPE that are empirically known to transfect exhibit the H_{II}^C phase, rather than the L_α^C structure found in complexes containing DOPC. Optical imaging showed that complex interactions with model cell membranes mimicking the early stages of transfection are structure-dependent.

Synchrotron SAXS scans of positively charged CL-DNA complexes for $\rho = 3$ are shown in Fig. 2A as a function of increasing Φ_{DOPE} in the DOPE-DOTAP CL mixtures along pathway I (*8*). [Here and below, ρ denotes the DOTAP/DNA weight ratio, Φ_{DOPE} is the weight fraction DOPE/(DOPE + DOTAP), and Φ_{DOPC} is the weight fraction DOPC/(DOPC + DOTAP).] The complexes are charged positively for $\rho > 2.2$ and negatively for $\rho < 2.2$, which indicates that charge reversal occurs when complexes are stoichiometrically neutral (with one positive lipid per negatively charged nucleotide base). At $\Phi_{DOPE} = 0.41$, SAXS scans of the lamellar L_α^C complex (Fig.

Materials Department, Physics Department, and Biochemistry and Molecular Biology Program, University of California, Santa Barbara, CA 93106, USA.

*Present address: Sektion Physik der Ludwig-Maximilians-Universität München, Geschwister-Scholl-Platz 1, 80539 München, Germany.

†Present address: Physikdepartment, Technische Universität München, Institut für Biophysik (E22), James Franck-Strasse, 85747 Garching, Germany.

‡To whom correspondence should be addressed.